

Core excitons in amorphous magnesium alloys*

John H. Slowik[†]

Department of Physics and Materials Research Laboratory, University of Illinois, Urbana, Illinois 61801

(Received 28 August 1973)

High-resolution photoabsorption spectra were obtained in the range 40–200 eV for Mg–group-V alloys. Sharp line structure was discovered for amorphous alloys of Mg–Bi and Mg–Sb near the photoabsorption threshold of the Mg $2p$ core level. These lines were strongest for compositions corresponding to the intermetallic compounds in the crystalline solid, and are thought to be due to the formation of core excitons. The positions and shapes of the exciton lines contain information about short-range screening, ionicity, and excited-state lifetime in the amorphous solids. Variation in the line shape of the threshold is described by a critical exponent, and appears to be continuous between compositions having insulating conductivity and compositions approaching metallic conductivity. This supports the idea that the metallic $L_{II,III}$ threshold is a remnant exciton singularity. Exchange interaction alters the relative strengths of the threshold doublet which originates in the spin-orbit splitting of the $2p$ initial state. This electron-hole exchange suggests a compact excitation wave function. Furthermore, for sufficiently long screening lengths the excitons sharpened enough to uncover additional structure, possibly due to higher-order members of an exciton series. The fact that excitons were not observed in crystalline alloys of Mg–Bi is attributed to a change in conductivity and to the nature of the critical exponent in the ordered phase.

I. INTRODUCTION

In amorphous solids, the circumstances for which one might expect to find sharp photoabsorption structure are not intuitively obvious. One might expect composition-dependent behavior in nondilute amorphous alloys to be only weakly dependent on small variations in alloy stoichiometry. In fact, sharp structure can occur which depends rather sensitively on stoichiometry, and which therefore can be used to probe into the nature of excited electron states in disordered systems in general. While the physical properties of tetrahedrally bonded semiconductors, chalcogen, and chalcogenide semiconductors have received considerable attention, few other systems have been extensively studied. Here we present high-resolution spectral measurements of the optical absorption due to electrons in the Mg–Bi and Mg–Sb alloy systems. For the amorphous alloys, sharp photoabsorption line structure is found in the soft-x-ray region, probably due to the formation of core excitons. Conductivity-dependent changes in the line shapes contain information about electronic properties and interactions in the amorphous and crystalline phases, including short-range screening, scattering phase shifts, and ionicities.

Resonances which may be due to exciton formation have previously been reported in the absorption spectrum of liquid Ga.¹ Excitons have been studied in liquid rare gases² and in solid Xe–Hg thin-film mixtures.³ Also, the infrared absorption edge of amorphous Se has a nonconducting component.⁴ Arguments which have been made against the likelihood of finding sharp exciton structure in amorphous solids⁵ pertain more to extended Wan-

nier or band-gap excitons. The x-ray excitons are shown to be compact. They are probably therefore less affected by disorder.

Among binary crystalline systems, Mg–Bi and Mg–Sb occupy a middle ground between typically metallic alloys and ionic crystals.⁶ The elements involved are essentially immiscible except for the formation of a single, thermodynamically stable, homogeneous intermetallic phase. This phase satisfies the formal $8 - N$ chemical valency rule if one ascribes to Bi a -3 valence state (which is not one of its commonly assigned valencies). Crystalline Mg_3Sb_2 (which we write $c\text{-}Mg_3Sb_2$) is a semiconductor with a band gap of about 0.8 eV.^{7–9} The data for Mg_3Bi_2 suggest that it is a semimetal in the crystalline phase.¹⁰ Simple electronic properties like the static dielectric constant and the Hall mobility remain unmeasured in $c\text{-}Mg_3Bi_2$, and only a few transport measurements have ever been made on $c\text{-}Mg_3Sb_2$.^{7–12}

Only narrow ranges of solubilities exist around 0, 60, and 100-at. % Mg. However, uniform metastable amorphous solids can be made at practically any composition. We used synchrotron radiation to scan the spectral response of these amorphous alloys from 40 to 200 eV. The advantages of synchrotron radiation as a probe of electron states has been amply documented.¹³ We paid particular attention to the region of photon energy around 50 eV, corresponding to photoexcitation of the Mg $2p$ core level, leaving a deep hole in the Mg $2p$ core. The “impurity” potential of this hole, as screened by the rest of the system, can bind the excited electron and form a “core exciton” or “x-ray exciton.” Evidence for such an excited state was

found in amorphous $\text{Mg}_x\text{Bi}_{1-x}$ (which we write $a\text{-Mg}_x\text{Bi}_{1-x}$), for values of x within a small range about $x = 0.6$.¹⁴ Excitons were also found in $a\text{-Mg}_x\text{Sb}_{1-x}$ where the screening length is longer, covering a wider range of compositions. In the Sb alloys it was possible to study the continuous transformation of exciton lines¹⁵ to the type of enhanced threshold previously seen in metals.¹⁶ In Sec. II we discuss the synthesis and characterization of thin films of these amorphous solids. In Sec. III there is a brief discussion of the experimental technique. Several new points which emerged in association with the present work are emphasized. Absorption coefficient data are presented and interpreted in Sec. IV.

The composition-dependent behavior of the conductivity, thermoelectric power, and temperature coefficient of resistivity in $a\text{-Mg}_x\text{Bi}_{1-x}$, suggests a Fermi level moving through a pseudogap.¹⁷ Electrical conductivity varies over more than five orders of magnitude in $a\text{-Mg}_x\text{Bi}_{1-x}$, and over more than eleven orders of magnitude in $a\text{-Mg}_x\text{Sb}_{1-x}$ as a function of composition x . By controlling composition of the amorphous solid, the electrical conductivity can be varied continuously through a range extending from a semimetallic or semiconducting value (10^0 and less than $10^{-6} \Omega^{-1} \text{cm}^{-1}$, respectively, at 80 K) to a typically metallic value ($10^5 \Omega^{-1} \text{cm}^{-1}$).^{10,17,18} One important implication of this widely variable conductivity is that by controlling stoichiometric composition of the alloys, screening length can be controlled simply by limiting the number of mobile carriers available. Information about crystalline and amorphous electronic properties is extracted from the conductivity- and order-dependent line shape in Sec. V. A parameter is suggested to quantitatively describe the strength of the exciton resonance at threshold.

II. SAMPLE PREPARATION

A. Synthesis of amorphous samples

The equilibrium phase diagrams for the Mg-Bi and Mg-Sb alloy systems¹⁹ show that these elements possess little mutual miscibility, except for the existence of intermetallic compounds Mg_3Bi_2 and Mg_3Sb_2 . The crystallized (equilibrium) solid, $\text{Mg}_x\text{Bi}_{1-x}$ or $\text{Mg}_x\text{Sb}_{1-x}$ for $0 \leq x \leq 1$, is therefore a polycrystalline mixture of two distinct phases, except at $x = 0, 0.6, \text{ and } 1$.

It is possible, however, to make uniform *amorphous* alloys $a\text{-Mg}_x\text{Bi}_{1-x}$ and $a\text{-Mg}_x\text{Sb}_{1-x}$ which are at least metastable. These amorphous alloys can be maintained amorphous and uniform as long as their temperature is kept below their composition-dependent crystallization temperature. They can be made over a range covering at least $0.2 \leq x \leq 0.8$

by vapor co-deposition of Mg and the heavy element. It was important to make samples of accurate and uniform stoichiometric composition, and also to keep them amorphous and stable through various stages of the experiment, because the electrical properties of the alloys depend on composition and the degree of order present.

Samples of the II-V alloys were prepared *in situ* for x-ray absorption spectroscopy by vapor deposition of 99.995% Mg and 99.999% Bi or Sb onto cold substrates in high vacuum. Typically an evaporation required about 15 min. The two components were coevaporated from separate resistance-heated sources. The ratio of the fluxes in the two evaporant beams was monitored with piezoelectric quartz crystals. The two sources were specially designed to have uniform time rates of evaporation. This allowed the evaporation rates to be controlled manually, without the benefit of any automatic feedback control,²⁰ as is needed for less sophisticated evaporation sources. Coevaporation is superior to evaporation from a single source because alloys cannot always be relied upon to evaporate stoichiometrically.

Ordinarily quartz crystals are used to measure deposited thickness.²¹ The adaptation shown in Fig. 1 allows the relative coevaporation rates to be controlled, so as to produce a uniform composition. The output frequency of the crystal oscillator was compared with a reference frequency of a variable-frequency oscillator (VFO) which initially was set at the same frequency as the crystal. These two outputs were fed into a mixer whose nonlinear element generated sum and difference frequencies. As evaporation proceeded, this difference frequency went from zero to a value which was proportional to the mass which had been deposited onto the crystal. This change in crystal mass was in turn proportional to the mass which had been deposited onto the sample by the evaporation source.

Both evaporation components were monitored by circuits of this type. The ratio of the two difference frequencies was displayed by feeding the difference frequencies into a Monsanto 100A counter-timer used in the ratio mode. An astable multivibrator was inserted into the Mg-monitoring half of the circuits to provide frequency division and thus increase the sensitivity of the counter-timer to nonstoichiometric coevaporation. During deposition, the ratio of the difference frequencies was kept constant as the frequencies themselves changed with progressive deposition, resulting in a sample of uniform composition. Judging by the observed stability of the evaporation sources and the measured stability of the coevaporation electronics and display ratio during actual coevaporation, the compositions of samples reported here are accurate and uniform to within 2-at. % Mg.

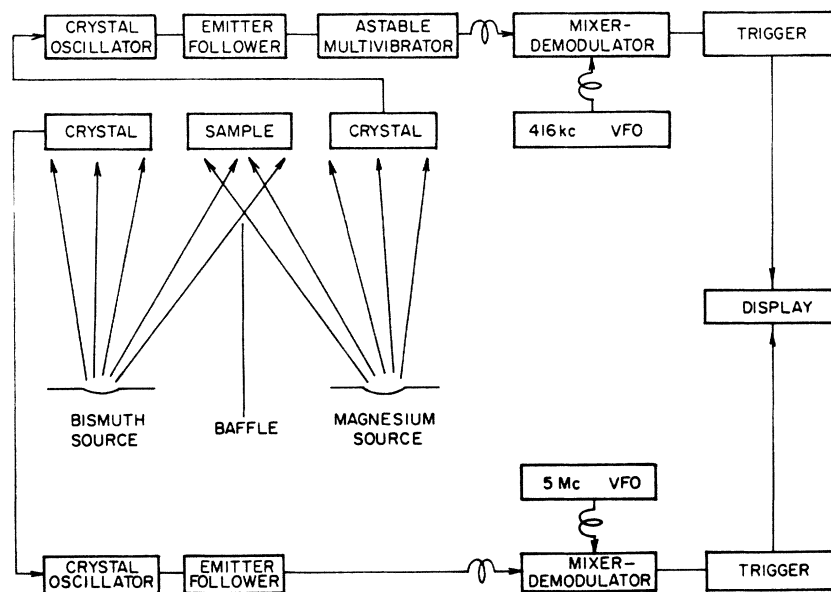


FIG. 1. Schematic diagram of electronics to monitor sample thickness and composition.

B. Characterization of the amorphous state

Unlike amorphous Si or Ge, details of possible short-range ordering are unknown in amorphous Mg-group-V alloys, except for the presumption that short-range stoichiometry is maintained. It has been suggested that strongly composition-dependent conductivity and thermopower imply "fairly-well-defined molecular groups"²² in liquid Mg_3Bi_2 . It is claimed that a disparity of atomic sizes is an aid to forming amorphous alloys.²³ However even elemental metals have been prepared in the amorphous state by lowering the substrate temperature sufficiently.²⁴ We were able to prepare amorphous II-V alloys by vapor deposition onto substrates below 100 K. This cooling was achieved principally by surrounding the thin-suspended-formvar substrate with a nearly 4π solid angle of liquid-nitrogen-cooled surfaces. This temperature was maintained during the spectroscopic measurements.

$\text{Mg}_x\text{Bi}_{1-x}$ alloys crystallize at temperatures ranging between 150–350 K.¹⁷ It has been observed that the conductivity of Mg_3Bi_2 rises by more than three orders of magnitude when amorphous samples crystallize.¹⁷ Some samples were prepared under identical geometry and evaporation conditions as used for spectroscopy, except that the formvar substrates were mounted on Teflon instead of copper. For $\alpha\text{-Mg}_3\text{Bi}_2$, the conductivity increased by a factor of 2.3×10^3 between 100 and 290 K. Most of this change occurred rapidly at 270 K, which is therefore identified as the crystallization temperature for Mg_3Bi_2 . If a weighted-average melting temperature is used, Mader's criterion for the amorphous to crystalline transition²³ predicts a crystallization temperature between 230–270 K.

The large change in conductivity shows that the films were amorphous as deposited. Also, the optical response was markedly different between low-temperature as-deposited films and low-temperature films that had been cycled up to room temperature and back. This alone implied that irreversible annealing had taken place.

Samples of both $\text{Mg}_x\text{Bi}_{1-x}$ and $\text{Mg}_x\text{Sb}_{1-x}$ whose absorption coefficients were measured at liquid-nitrogen temperature were also examined by electron microprobe, transmission electron microscope, and electron diffraction at room temperature. Electron-microprobe examination showed that the compositions of the films were uniform over the physical dimensions of the films, down to a resolution of 1 μm . Electron diffraction patterns showed that $\text{Mg}_x\text{Bi}_{1-x}$ alloys were generally crystallized at room temperature, although sometimes just barely (diffuse Mg_3Bi_2 intermetallic compound rings, plus sharp rings of any excess metal). Sizes of the popcorn-shaped crystallites, as measured in the transmission electron microscope at room temperature, depended on composition. The crystallinities were as large as 7×10^3 Å in diameter for $x=0.4$, and typically around 100 Å in diameter for $x=0.6$. Mg-rich alloys pose a puzzle. It seems strange that alloys which are 90-at.% Mg should have an annealing temperature so high as 350 K¹⁷ at the same time that pure metals are so notably difficult to make amorphous. It seems at least plausible that the deposited thin film of such an alloy might be composed of crystallites whose tiny size is at the fuzzy boundary of being "amorphous." Then, as Ferrier and Herrell suggest,¹⁷ the less pronounced annealing may simply be an increase in grain size. For Mg-rich $\text{Mg}_x\text{Bi}_{1-x}$ alloys, actual

grain sizes were somewhat obscured by surface irregularity, but appeared to be less than 100 Å.

Unlike the Mg_xBi_{1-x} alloys, Mg_xSb_{1-x} alloys remain amorphous at room temperature. A crystallization temperature of 450 K is cited for Mg_3Sb_2 .¹⁰ It was verified that samples which had actually been subject to x-ray absorption spectroscopy at 100 K, were still amorphous at room temperature when examined by electron diffraction. These showed only the broad halo patterns typical of amorphous solids, and no sharp rings. Electron micrographs showed no patterns identifiable as crystallites. No crystalline samples of Mg_xSb_{1-x} alloys were studied in the present work.

III. X-RAY ABSORPTION SPECTROSCOPY

Soft-x-ray absorption spectroscopy (XAS), using synchrotron radiation from a synchrotron or an electron storage ring, is becoming a well established technique.^{13,25-27} The 240-MeV electron storage ring at the University of Wisconsin Physical Science Laboratory was used as the source of synchrotron radiation in this experiment. The XAS apparatus and data gathering system is essentially unchanged from the system described elsewhere,²⁷ except that the grazing incidence optics have been rotated 90° so that the electric vector of the polarized light lies parallel to the reflecting and diffracting surfaces. A coevaporation chamber was inserted into the system to make binary-alloy samples *in situ*. The light transmitted by the sample was analyzed in a 2-m grazing-incidence spectrometer using a 1200-line/mm grating which is blazed for a first-order maximum near 100 Å. The spectrometer bandwidth was better than 0.02 eV for photon energies around 50 eV. A Bendix channeltron detector was used to count photons selected by the exit slit.

In the extreme ultraviolet, the deeper initial-state electron energy levels are narrow in energy width. The energy distribution of the absorption spectrum often closely follows the energy distribution of one-electron final states.²⁸ There is sometimes additional structure associated with final-state interactions or excitons.

The binding energy of an electron in the $2p$ core level of Mg is about 50 eV. In a crystal the advantage of using such a deep level as an initial state is that such a level has a sharply defined energy. In an amorphous solid one must consider the possible broadening effect of local fields due to variable nearest neighbor coordination. The sharpness of the spectra presented in Sec. IV suggests that such broadening is negligible.

There is uncertainty in the values of the linear absorption coefficients on the order of 25%. This is principally caused by scattering due to surface roughness of the sample, and by uncertainty in the

value and uniformity of film thickness d . All films had relatively smooth surfaces as deposited. A few samples, however, showed progressively worse surface roughness as a function of time, as measured by their percent transmission to the synchrotron radiation beam. The development of roughness could be measured and compensated for in calculating $\alpha(\omega)$. This effect was not seen in Mg-Sb alloys. In Mg-Bi alloys it occurred only in films less than 170 Å thick, and may be caused by the formation of islands. All data from rough-surfaced ultrathin films was disregarded.

IV. EXPERIMENTAL RESULTS

A. Preliminary considerations

Both Mg_3Bi_2 and Mg_3Sb_2 form hexagonal crystals of a type which suggests ionic compounds, anti- La_2O_3 .²⁹ The space group is $C\bar{3}m (D_{3d}^3)$. The unit cell of this structure is pictured in Fig. 2 for the bismuthide. The atoms which comprise the unit cell are labeled in the upper drawing. In the lower drawing the numbers give the heights of various atoms above the base of the unit cell, in units of lattice spacing c_0 .²⁹ These Π -V alloys probably crystallize into this form because of the disparate sizes of the constituent atoms. Among other alloys of Mg with group-V elements the crystal structure is cubic Mn_2O_3 type,²⁹ although Mg_3As_2 is also hexagonal anti- La_2O_3 above 1000 °C.³⁰ Note that Mg_3Bi_2 and Mg_3Sb_2 have high-temperature crystalline phase transitions. For these alloys, reference here to the crystalline phase will always mean the room-temperature α -phase.

The lack of mutual miscibility between Mg and Bi at any composition other than the compound formed according to the $8-N$ valence rule, Mg_3Bi_2 , suggests an ionic description. Although c - Mg_3Bi_2 is probably a semimetal,¹⁰ let us assume charge transfer for the sake of constructing a ladder diagram of the energy levels as a lowest

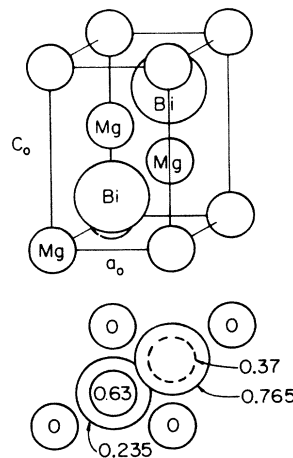


FIG. 2. Unit cell of α - Mg_3Bi_2 . In this phase the crystal is hexagonal anti- La_2O_3 type. The basis atoms are labeled in the upper drawing. The lower drawing is a top view of the same unit cell, and the numbers give the heights of various atoms above the base of the unit cell, in units of c_0 (from Ref. 29).

approximation to the band structure. That the arrangement of levels for crystalline and amorphous material might be similar, is suggested by recent electron-spectroscopy-for-chemical-analysis (ESCA) studies of *a*- and *c*-GeTe,³¹ where considerable changes in long- and short-range order do not significantly alter either the valence or core density of states.

If Mg^{2+} and Bi^{3-} ions are placed on the basis sites of the crystal lattice in Fig. 2, the Madelung potential of a Bi ion at either of the equivalent sites is roughly -35 eV when evaluated by direct summation for electrically neutral surrounding spheres. The Mg ions are distributed between two nonequivalent sites, but the weighted average Madelung potential for an Mg ion must be $\frac{2}{3}$ that of a Bi ion, since the Mg^{2+} sublattice is bound to the Bi^{3-} sublattice. The Madelung potential for Mg ions is thus about -23 eV.

The difference between the vacuum level and the Mg $2p$ level in ionic Mg_3Bi_2 is the 80.12-eV ionization potential of Mg^{2+} (Ref. 32) plus the -23 -eV lattice binding energy. We observe that the position of the delayed $5d \rightarrow nf$ spectral resonance structure shifts by about 0.42 eV in going from *c*-Bi to Bi in *c*- Mg_3Bi_2 . Therefore, in constructing the ladder diagram for *c*- Mg_3Bi_2 , we shift the position of the $5d$ level as determined by ESCA in

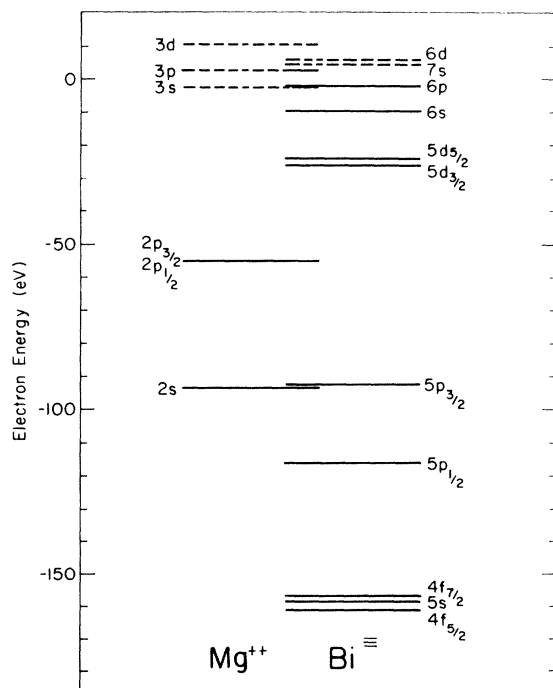


FIG. 3. Energy-level ladder diagram for Mg_3Bi_2 . The compound was assumed to be ionic. A more accurate picture would show the upper levels broadened into bands.

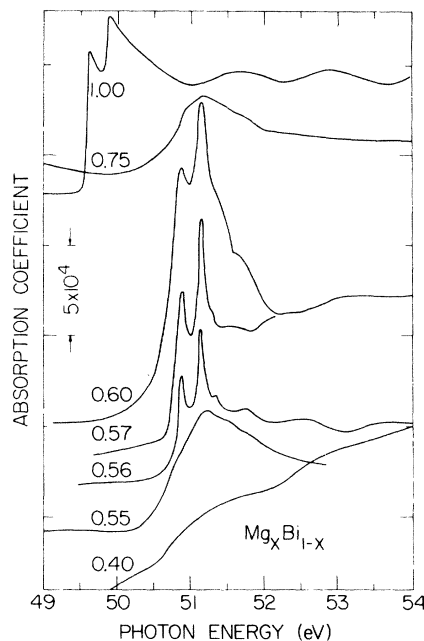


FIG. 4. Absorption coefficient versus photon energy for $\text{Mg}_x\text{Bi}_{1-x}$ at 100 K. Each curve is labeled by composition x . All samples were amorphous except for Mg metal, $x=1.00$, which was crystalline. The same scale applies to all spectra, but the curves have been shifted vertically for clarity. For comparison, the absorption coefficients at 50 eV, in units of 10^5 cm^{-1} , for decreasing x were 1.0, 1.7, 2.0, 2.5, 2.2, 4.9, and 5.6.

pure Bi (Ref. 33) by a similar amount. The resultant Mg $2p$ and Bi $5d$ level placement is as shown in Fig. 3. The placement of the remaining levels relative to these two is as determined spectroscopically³² or by ESCA.³³ The $j=\frac{1}{2}$, $\frac{3}{2}$ components of the Mg $2p$ level appear as a single level due to the scale used. Note that the $2p$ level is well isolated in energy from the next levels above and below it.

In Mg metal the $2p$ core level is spin-orbit split into $j=\frac{1}{2}$, $\frac{3}{2}$ levels. When sufficiently energetic photons excite the $2p$ electrons to the Fermi surface, the absorption spectrum clearly shows two excitation thresholds whose separation we measure as 0.273 ± 0.01 eV. At the top of Fig. 4 is a composite absorption spectrum for thin films of Mg metal, taken from our data and that of Kunz *et al.*,¹⁶ to illustrate this point. Because the initial state is split, the absorption spectrum is a superposition of two spectra, either of which is a first approximation to the band density of unoccupied states. In addition, there is a many-body enhancement of the threshold itself, and the effects of nonconstant matrix elements and decreasing oscillator strength above threshold. These parts of the absorption spectrum corresponding to excitation from the $j=\frac{1}{2}$,

$\frac{3}{2}$ levels of the $2p$ core are referred to as L_{II} and L_{III} respectively, and the total $2p$ photoexcitation threshold is referred to as the $L_{II,III}$ edge. The intensities of the $L_{II,III}$ component spectra, as measured above the background absorption from higher-lying states, are proportional to the statistical weights of the levels, $2j+1$. The ratio of the intensities is $I(L_{III})/I(L_{II})=2$.

The other spectra in Fig. 4 are for $a\text{-Mg}_x\text{Bi}_{1-x}$ alloys, and each is labeled with the appropriate value of x . For these spectra, the ratio of the two components of the threshold differs from 2. When Mg atoms form compounds with other elements, there may be increased overlap between the wave functions of the excited electron and the core hole, so that the exchange energy is appreciable and the $j=\frac{1}{2}, \frac{3}{2}$ designation may be inappropriate for distinguishing the excited eigenstates. This was pointed out by the work of Onodera and Toyozawa³⁴ where they applied atomic intermediate coupling to the solid state. For a p -like initial state and an s -like final state, there are four possible excited states of the system, but only two can be excited optically, just as in the jj coupling limit. These are designated A and C , and are such that they become the $j=\frac{1}{2}, \frac{3}{2}$ states, respectively, in the limit of zero electron-hole exchange energy. Transitions to the states A and C are not equally allowed. The transition probabilities depend on the relative admixtures of singlet states, which in turn depend on the magnitude of the exchange energy Δ relative to the spin-orbit splitting λ ,³⁴

$$I_C/I_A = \tan^2(\gamma - \phi) \quad , \quad (1)$$

where $\gamma = \arctan \sqrt{2}$, and $\phi = \frac{1}{2} \arctan [(2\sqrt{2}\Delta/\lambda)/(3 - \Delta/\lambda)]$. The splitting of the A, C doublet is ΔE , where

$$\Delta E/\lambda = [(\Delta/\lambda - \frac{1}{3})^2 + \frac{8}{9}]^{1/2} \quad . \quad (2)$$

For positive exchange energy $I_C/I_A < 2$. We have reported such alteration of the intensity ratio in resonances observed in amorphous alloys of Mg-Bi and Mg-Sb,¹⁵ and it has been reported by Rabe *et al.* in crystalline Mg halides.³⁵

The data which we present for the Mg-Bi and Mg-Sb alloys is for samples with thicknesses ranging from 140 to above 500 Å thick, and is regarded as characteristic of the bulk material for the lowest-order exciton and the band density of states. The nature of the exciton resonance is independent of film thickness within this range. Exciton strength in samples of Mg-Sb alloy with thickness less than 100 Å appeared to decrease with decreasing thickness. No extensive study of excitons in ultrathin films was undertaken.

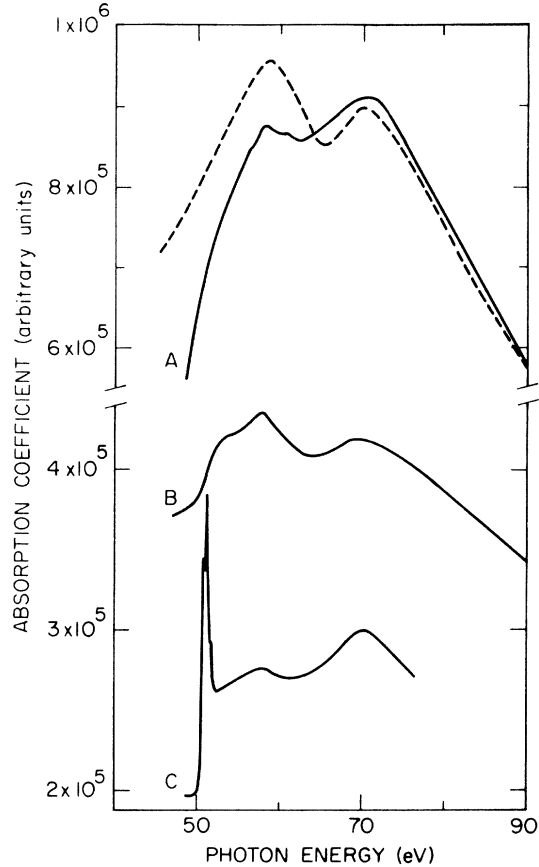


FIG. 5. Absorption spectra of Bi and Mg_3Bi_2 . (A) Bi deposited and measured below 100 K, (B) microcrystalline Mg_3Bi_2 annealed to 300 K, (C) amorphous Mg_3Bi_2 deposited and measured below 100 K, showing sharp excitons. The dashed line is the spectrum of Bi reported in Ref. 36. A split vertical scale is used, and curve B has been shifted upward for clarity.

B. Amorphous and crystalline $\text{Mg}_x\text{Bi}_{1-x}$

The broad features of absorption spectra of a - and c - Mg_3Bi_2 are dominated by the delayed $5d-nf$ resonance structure of the Bi atom. This can be seen in Fig. 5 which compares the spectra of Bi and Mg_3Bi_2 for both amorphous and crystalline forms. At the top is the spectrum of c -Bi (dashed line) as measured by Haensel *et al.*³⁶ Below are our spectra for (a) Bi deposited and measured below 100 K, (b) c - Mg_3Bi_2 , and (c) a - Mg_3Bi_2 . The broad structure has a characteristic width of about 20 eV and is easily separable from the sharp absorption structure which appears near 51-eV photon energy in the Mg-Bi alloys, associated with the excitation of the Mg $2p$ electrons (see Fig. 3).

The sharp resonances in a - $\text{Mg}_x\text{Bi}_{1-x}$ are shown on a magnified scale in Fig. 4 for a variety of compositions, $x=0.40, 0.55, 0.56, 0.57, 0.60,$ and 0.75 . Also shown is the spectrum of c -Mg metal,

$x=1.00$. All spectra are drawn to the same scale, but the spectra have been shifted vertically for clarity of display. These doublet resonances were strongest for those amorphous alloys whose compositions were closest to $x=60$ -at. % Mg, the composition corresponding to the intermetallic compound. The resonance is believed to be due to the creation of an exciton for the following reasons. It is clear that the initial state is the Mg $2p$ level, because the resonances correspond to the absorption of photons whose energies are near 51 eV, and furthermore the resonances are doublets whose exchange modified splitting is comparable to the 0.273 ± 0.1 eV spin-orbit splitting of the Mg $2p$ core, cited earlier. The resonances cannot be due to transitions to an impurity level, since they are of considerable strength, comparable to the Mg step height, and furthermore because the resonances are present only for the process which creates a hole in the Mg $2p$ core level. The sharpness of the resonances and their strong dependence of intensity upon composition make it unlikely that they could be due to a critical point effect in the final states. In fact the reduced-zone expression of band structure should be at best only approximately adaptable to amorphous solids.

These excitons are of a specific type, called core excitons or x-ray excitons. They are bound electron-hole pairs where the hole is in a deep (Mg $2p$) level, and the electron is well localized about the Mg atom which bears the nonmobile hole. The compactness of the exciton can be seen from the weighting of the threshold doublet structure, where the ratio of intensities I_C/I_A was 0.8 ± 0.1 for α -Mg₃Bi₂, instead of 2 as for Mg. This implies considerable exchange interaction due to overlap. According to Eq. (1), the exchange energy must be nearly half as large as the 0.27-eV spin-orbit splitting of the $2p$ initial levels.

When x differs from 0.6 the excitons became weaker, due to screening of the potential which binds the electron and hole of form the exciton.¹⁵ For an impurity potential of the type³⁷

$$\delta U = (e^2/\epsilon r) e^{-\lambda r}, \quad (3)$$

the classical screening length $1/\lambda$ is given by

$$1/\lambda = (\epsilon/4\pi e^2 N)^{1/2}, \quad (4)$$

where ϵ expresses the screening due to the ion cores, and N is the density of carriers per unit energy which are effective in screening. Conductivity as a function of composition (Fig. 8 in Ref. 17) indicates a strong dependence of N on composition, assuming the mobility does not change dramatically. The mechanism for electrical conductivity in these alloys is not yet clear. Possibilities include extended state or hopping transport either near a mobility edge or at the Fermi level. The excitons

in α -Mg_xBi_{1-x}, which are strong and sharp at $x=0.6$, are broader and weaker for $x=0.55$ and 0.65 , where the conductivity $\sigma \approx 100 \Omega^{-1} \text{cm}^{-1}$. This is near to the value for separating metallic conductivity from hopping via localized states.⁵ If one places the Fermi level near the edge of the pseudogap, the density of states there could hardly exceed $N(E_F) \sim 10^{21} \text{cm}^{-3} \text{eV}^{-1}$ and still leave a pseudogap. Using this value in Eq. (4) gives an estimated lower limit for the screening length of 2–7 Å, for choices of ϵ between 1 and 9. Since the excitons begin to be screened at $x=0.55$ and 0.65 , this would, in turn, be an estimate of the exciton radius. Note that a lower estimate of N for $x=0.55$ or 0.65 leads to a larger exciton radius. At the stoichiometric composition, $x=0.6$, the conductivity is between 0.1 – $1.0 \Omega^{-1} \text{cm}^{-1}$. Thus at $x=0.6$ the screening length is expected to be more than ten times larger so that the electron and hole should remain bound via the potential, Eq. (3). Accordingly the absorption resonances in Fig. 4 were strong and well defined around $x=0.6$, the stoichiometric composition corresponding to the intermetallic compound.

The broadening which accompanied decreasing oscillator strength for $x \neq 0.6$ was asymmetric, being larger in the direction of the higher transition energies. Even at $x=0.6$ the resonances appeared to be asymmetric, although they did become sharp enough to uncover additional structure which may be an envelope of higher-order members of an exciton series. Figure 6 shows the $\alpha_C(\omega)$ component absorption spectrum of α -Mg₅₇Bi₄₃. To get this spectrum, the background was subtracted from the total absorption spectrum, leaving the absorption associated only with excitation of the Mg $2p$ electrons:

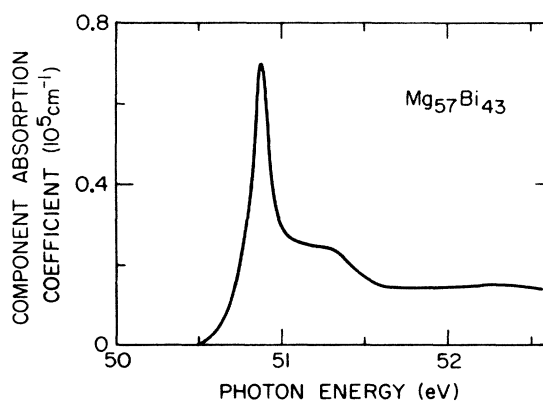


FIG. 6. Component absorption spectrum of α -Mg₅₇Bi₄₃. After background absorption was subtracted from the threshold spectrum, the A and C component transitions were separated. Only the $\alpha_C(\omega)$ component spectrum is pictured above. Sample was amorphous and at 100 K.

$$I(\omega) = \alpha_C(\omega) + \alpha_A(\omega) \quad (5)$$

This was then decomposed into $\alpha_C(\omega)$ and $\alpha_A(\omega)$ component spectra, by computer analysis and plotting. The two component spectra were assumed to be related by

$$\alpha_C(\omega) = (I_C/I_A)\alpha_A(\omega + \Delta E) \quad (6)$$

where I_C/I_A is the intensity ratio in Eq. (1). The values of I_C/I_A and ΔE were varied as parameters to find the best fit.

The energy difference between the threshold peak and higher energy structure was 0.4 ± 0.1 eV for those compositions near $x = 0.6$ which showed evidence of higher-order excitons. The simple Elliott exciton theory^{38,39} can be modified to estimate an upper limit for the radius of an exciton. In the simple theory excitons are found below the conduction band edge E_c , at energies E_n ,

$$E_n = E_c - \mu^* R_0 / n^2 m_e \epsilon_n^2 \quad (7)$$

where R_0 is the hydrogen rydberg unit $R_0 = e^4 m_e / 2\hbar^2$, and μ^* is the reduced mass $m_e^* m_h^* / (m_e^* + m_h^*)$. The radius of the n th exciton is

$$r_n = n^2 \epsilon_n a_0 m_e / \mu^* \quad (8)$$

where a_0 is the Bohr radius $a_0 = \hbar^2 / e^2 m_e$. For a Wannier (large-radius) exciton, ϵ_n is just the static dielectric constant ϵ_s . For a compact exciton, ϵ_n depends on the exciton radius r_n and the effective mass of the electron m_e^* . Assuming that the effective mass of the core hole is infinite, according to Haken ϵ_n is given by⁴⁰

$$\frac{1}{\epsilon_n} = \frac{1}{\epsilon_s} + \frac{1}{2} \left(\frac{1}{\epsilon_\infty} - \frac{1}{\epsilon_s} \right) \exp \left[-r_n \left(\frac{2m_e^* \omega_{LO}}{\hbar} \right)^{1/2} \right] \quad (9)$$

where ϵ_∞ is the high-frequency dielectric constant and ω_{LO} is the frequency of the longitudinal-optical phonon. For Wannier excitons the energy difference between the first two exciton series members ($n = 1, 2$) can be found from Eq. (7) and used to eliminate ϵ_n in Eq. (8):

$$r_n(\epsilon_s) = \frac{n^2 a_0}{2} \left(\frac{3R_0 m_e}{(E_2 - E_1) \mu^*} \right)^{1/2} \quad \text{Wannier.} \quad (10)$$

Since ϵ_n depends on n for a compact exciton,⁴¹ the Wannier radius in Eq. (10) is an upper limit on the true exciton radius,

$$r_n(\epsilon_n) \leq r_n(\epsilon_s) \quad (11)$$

where we have assumed $\epsilon_n \leq \epsilon_s$ from Eq. (9). For the core exciton in $a\text{-Mg}_x\text{Bi}_{1-x}$ for x near 0.6 we find

$$r_1 \leq (2.7 \text{ \AA}) f_e^{1/2} \quad (12)$$

where $f_e = m_e / m_e^*$. Thus, for those compositions where the exciton line is strong, the exciton radius may indeed be less than the 2–6-Å screening

length, which we have earlier estimated from the conductivity of those compositions where the resonance began to weaken.

The identification of the higher-energy structure as an envelope of $n > 1$ excitons should still be regarded as tentative however. The higher-energy peak may be caused by a different process. It could conceivably be a multiple excitation, where creation of the core exciton is accompanied by the excitation of an electron across the pseudogap. The separation between the exciton resonance and the higher structure is 0.4 ± 0.1 eV, which is about the width of the pseudogap minimum estimated by Ferrier and Herrell from thermoelectric measurements, using a model in which the density of states is composition independent.¹⁰ However, it has been argued that such a multiple process would be weak even when the two excited electrons originate from the same energy band.⁴² If the higher-energy structure really is an $n > 1$ exciton envelope, then one must ask what is the effect of having the exciton binding energy so large that the exciton approaches the edge of the density of extended states in the valence band. There could be interactions or competing processes which interfere with each other.

Some samples were partially annealed at a temperature below the crystallization temperature, and then returned to below 100 K. No differences larger than the 0.02-eV instrument spectral bandwidth were seen between exciton linewidths at these extremes of temperature (probably 100–250 K). The reason is probably that the theoretical linewidth, which is proportional to $T^{1/2}$, should involve an effective temperature which includes both the real temperature and the high density of lattice imper-

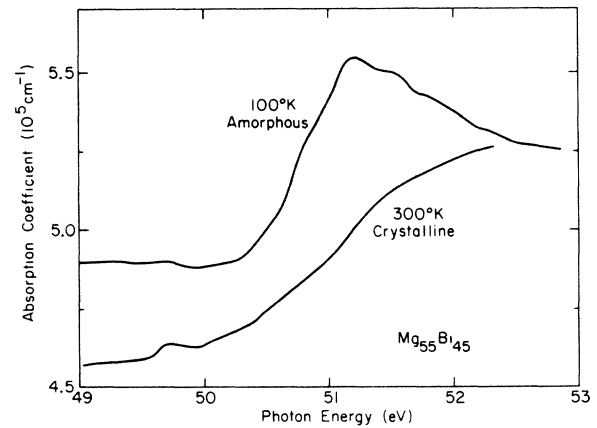


FIG. 7. Absorption spectra of $\text{Mg}_{55}\text{Bi}_{45}$. The amorphous spectrum was taken below 100 K and shows the partially screened exciton. The crystalline spectrum was taken at 300 K and shows only monotonically rising absorption, and does not change upon recooling.

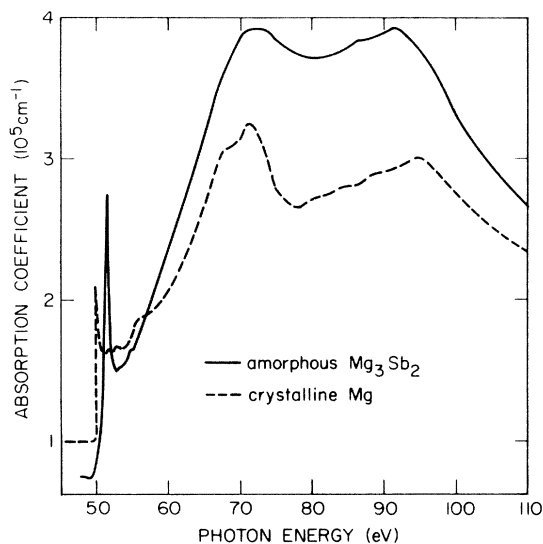


FIG. 8. Absorption spectra of α - Mg_3Sb_2 and c -Mg. The solid line is the spectrum of α - Mg_3Sb_2 deposited and measured below 100 K. The dashed line is the spectrum for c -Mg, measured at 100 K.

fections in the amorphous solid, as suggested by Toyozawa.⁴³

When α - $\text{Mg}_x\text{Bi}_{1-x}$ was heated to above its crystallization temperature the excitons disappeared, and did not reappear upon recooling. This behavior was shown in Fig. 5 for the sharpest excitons, $x=0.6$. At $x=0.55$, where the excitons were weaker and broader, the behavior was the same, as is shown in Fig. 7. The structure at 49.7 eV is a trace of the Mg $L_{\text{II,III}}$ edge. The spectra for all crystallized samples of $\text{Mg}_x\text{Bi}_{1-x}$ for $0.4 \leq x \leq 0.8$ were qualitatively the same. This was not surprising since the equilibrium phase diagram¹⁹ leads one to expect phase separation. For $x \geq 0.8$ the Mg $L_{\text{II,III}}$ edge became more prominent, due to increased precipitation of Mg crystallites. For $x < 0.4$ the Bi $5d \rightarrow nf$ resonance overwhelmed the remaining traces of Mg structure.

C. Amorphous $\text{Mg}_x\text{Sb}_{1-x}$

There are two important differences between the positions of crystalline energy levels in Mg_3Sb_2 and Mg_3Bi_2 . The Sb $4d$ levels replace the Bi $5d$ levels since Sb is one row higher in column V of the Periodic Table. These $4d$ levels lie about 10 eV lower, so that the delayed $4d \rightarrow nf$ resonance is shifted about 10 eV toward higher photon energy, away from the Mg $2p$ threshold structure. Accordingly, the α - Mg_3Sb_2 absorption spectrum was dominated by the Mg absorption, as can be seen from Fig. 8, which compares the wide-range spectra which we obtained for α - Mg_3Sb_2 (solid line) and c -Mg (dashed line). There is increased background absorption

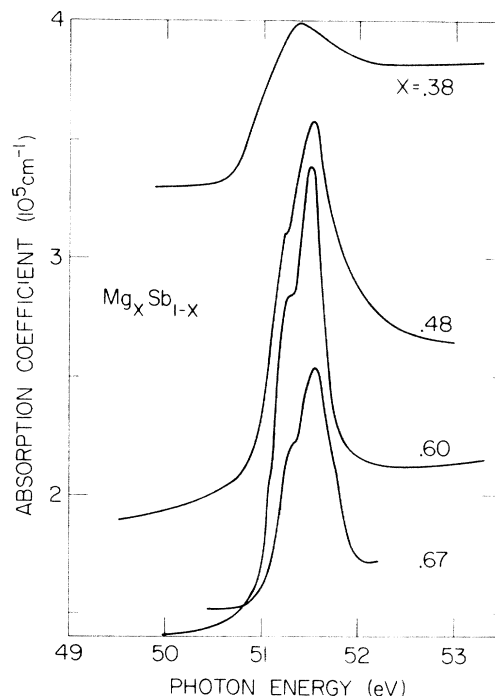


FIG. 9. Absorption coefficient vs photon energy for α - $\text{Mg}_x\text{Sb}_{1-x}$. Each curve is labeled by composition x . All samples were deposited and measured below 100 K.

between 60 and 100 eV in α - Mg_3Sb_2 due to the structureless Sb $4d \rightarrow nf$ delayed resonance.

The second difference concerns the assumption

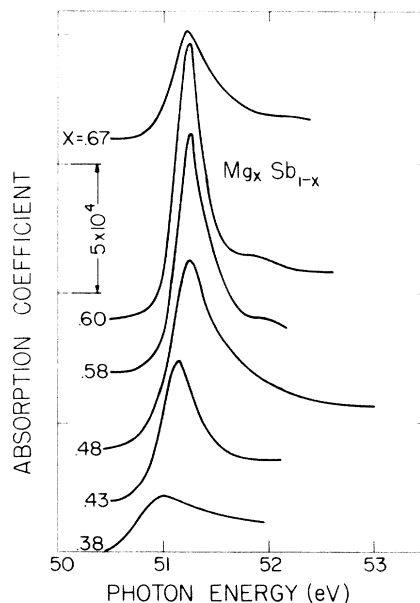


FIG. 10. Component absorption spectra for α - $\text{Mg}_x\text{Sb}_{1-x}$. Spectra were obtained in the same way as Fig. 6. These spectra represent one component of the threshold doublet. Each curve is labeled according to composition x . All samples were deposited and measured below 100 K.

that Mg_3Bi_2 and Mg_3Sb_2 are ionic for the purpose of estimating energy level placement (Fig. 3). We drew the Bi 6*p* level as a solid line to indicate that it would be filled, and the Mg 3*s* level as a dashed line to indicate it would be empty, in accord with a closed shell model, and ignored the fact that these levels should actually be replaced by broad solid-state bands. Even in the absence of electrical data, the overlap of these levels suggests that Mg_3Bi_2 is not very ionic. In Mg_3Sb_2 on the other hand, the assumption is more self-consistent since the same procedure leads to placing the Sb 5*p* level lower than the Mg 3*s* level by nearly 5 eV. We find that the unoccupied Sb 6*s* level, which replaces the Bi 7*s* level, overlaps the Mg 3*s* level. Whereas the electron part of the exciton wave function may be expected to have strong *s-p* admixture in the Bi alloys, more *s*-like dominance may be expected in the Sb alloys, which means more 2*p-s* oscillator strength for the threshold transition.

Figure 9 shows absorption spectra of $a\text{-Mg}_x\text{Sb}_{1-x}$ for several compositions: $x = 0.38, 0.48, 0.60,$ and 0.67 . Compared to the spectra for $a\text{-Mg}_x\text{Bi}_{1-x}$, these spectra were (i) more broadened for compositions near $x = 0.6$, (ii) further shifted away from the threshold in pure Mg, toward higher photon energy, (iii) stronger in threshold oscillator strength, and (iv) strong for a considerably larger concentration of the group-V element. Differences (i)-(iii) are discussed below. The last-mentioned difference is easily understood in terms of the screening argument advanced earlier. The conductivities of amorphous Bi alloys and amorphous Sb alloys are similar for $x > 0.6$, but the conductivity for $x < 0.6$ is orders of magnitude lower in $a\text{-Mg}_x\text{Sb}_{1-x}$ (Fig. 3 in Ref. 10). The Coulomb potential [Eq. (3)] should be screened by fewer free carriers in the Sb alloy, even if the mobility were two orders of magnitude less in the Sb alloy. Therefore, the screening length [Eq. (4)] is longer so that the excitons remain relatively stable in Sb-rich amorphous alloy.

Before discussing further the composition depen-

dence of the exciton threshold in $a\text{-Mg}_x\text{Sb}_{1-x}$, it is useful to eliminate the doublet nature of the threshold by separating the $\alpha_c(\omega)$ and $\alpha_A(\omega)$ components of the $\alpha(\omega)$ absorption spectra. This procedure was discussed above, Eqs. (5) and (6). Figure 10 shows the resolved $\alpha_c(\omega)$ component spectra for $a\text{-Mg}_x\text{Sb}_{1-x}$ for compositions $x = 0.38, 0.43, 0.48, 0.58, 0.60,$ and 0.67 . The values of the intensity ratio I_C/I_A and the doublet splitting ΔE which gave the best fit are listed in Table I, together with the exchange energy Δ and spin-orbit splitting of the Mg 2*p* level as calculated from Eqs. (1) and (2). Also listed are values for $a\text{-Mg}_{57}\text{Bi}_{43}$ and $a\text{-Mg}_{60}\text{Bi}_{40}$, but these values are less reliable since the resolution of the sample preparation technique was about 2-at. % Mg, and the excitons change more rapidly with x in Mg-Bi alloys.

For x near 0.6 in the Sb alloys, there was again a trace of higher-energy structure, perhaps an $n > 1$ exciton envelope. However, even in the $\alpha_c(\omega)$ spectra it was only poorly resolved. As before, the spectra for $x \neq 0.6$ became more broadened, with the broadening being asymmetrically emphasized toward higher transition energies. Since the calculated values of exchange energy in Table I were comparable for Sb alloys and Bi alloys, the exciton is probably similarly compact in $a\text{-Mg}_x\text{Sb}_{1-x}$, although greater broadening suggests a shorter lifetime.

Unlike $\text{Mg}_x\text{Bi}_{1-x}$, the conductivity trough at $x = 0.6$ persists in $c\text{-Mg}_x\text{Sb}_{1-x}$. We did not prepare samples of $c\text{-Mg}_x\text{Sb}_{1-x}$, nor did we study the temperature dependence of the exciton line width in $a\text{-Mg}_x\text{Sb}_{1-x}$, since no variation was observed in the similar $a\text{-Mg}_x\text{Bi}_{1-x}$ system beyond the 0.02-eV instrument resolution.

The infrared absorption spectrum of $a\text{-Mg}_3\text{Sb}_2$ was measured at room temperature using a 250-Å-thick sample. The spectrum, Fig. 11, showed no trace of any exciton resonance. Even in such a thin sample, it should be possible to create an exciton without interaction with the surface, provided

TABLE I. Threshold data for Mg and amorphous alloys of Mg with Bi and Sb. Values for the intensity ratio and the doublet splitting are those that give the smoothest $\alpha_c(\omega)$. From this information, the exchange and spin-orbit splitting were calculated.

Composition	Intensity ratio I_C/I_A	Doublet splitting ΔE (eV)	Exchange energy Δ (eV)	Spin-orbit splitting λ (eV)
Mg	2	0.273	0	0.273
$a\text{-Mg}_{57}\text{Bi}_{43}$	0.95	0.27	0.10	0.29
$a\text{-Mg}_{60}\text{Bi}_{40}$	0.8	0.28	0.16	0.29
$a\text{-Mg}_{38}\text{Sb}_{62}$	0.51	0.3	0.2	0.3
$a\text{-Mg}_{43}\text{Sb}_{57}$	0.58	0.29	0.17	0.30
$a\text{-Mg}_{48}\text{Sb}_{52}$	0.70	0.28	0.15	0.29
$a\text{-Mg}_{53}\text{Sb}_{47}$	0.71	0.28	0.14	0.29
$a\text{-Mg}_{60}\text{Sb}_{40}$	0.70	0.27	0.15	0.29
$a\text{-Mg}_{67}\text{Sb}_{33}$	0.53	0.28	0.18	0.3

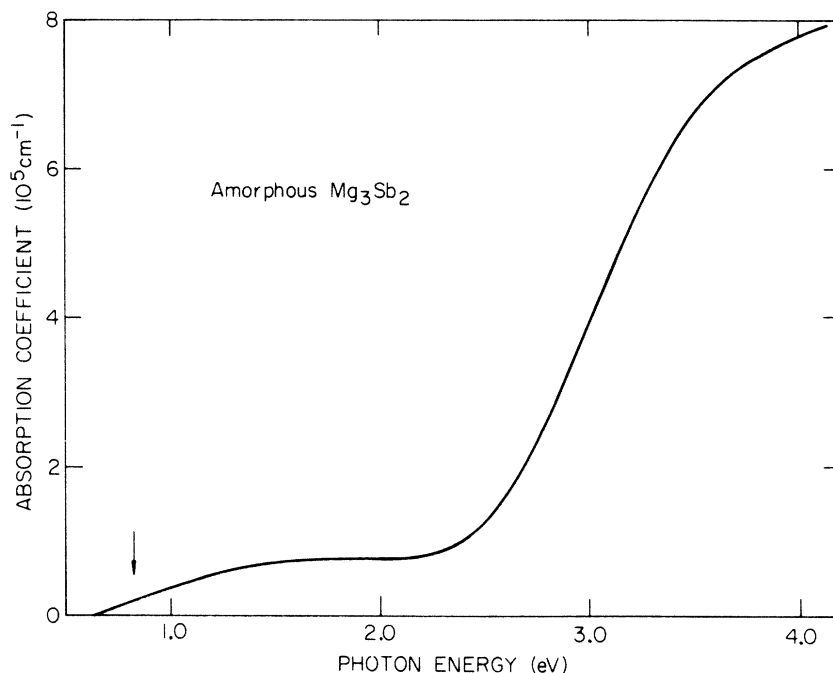


FIG. 11. Absorption spectrum of α - Mg_3Sb_2 in the infrared and visible regions. The position of the band gap in crystalline material, marked with a vertical arrow, is 0.82 eV according to Ref. 9.

its radius were less than $\sim 60 \text{ \AA}$. We observe only a gradual onset of absorption beginning at about 0.6 eV. Compare this to the crystalline band gap of 0.82 eV,⁹ which is marked by an arrow in the figure. It is likely that the valence-band hole wave function is more extensive than that of the core hole. It should interact more strongly with, and have greater probability to be scattered by, the conduction electrons. Measurements made at lower temperature would not necessarily lead to the observation of an exciton resonance, since there would still remain the high effective temperature associated with disorder.⁴³ If a band-gap exciton forms, it lacks the stability of the core exciton, which is probably attributable to its compactness.

Thicker samples would have to be studied to explore whether there is a nonzero density of localized pseudogap states below 0.6 eV in α - $\text{Mg}_x\text{Sb}_{1-x}$. On the basis of electrical measurements it has been suggested that this density is negligible and that the amorphous alloy is an extrinsic semiconductor.¹⁰

V. DISCUSSION

A. Critical exponent

Mahan was the first to suggest that exciton states do exist in degenerate semiconductors and metals, and that absorption threshold enhancements arise from exciton states as modified by interaction with the Fermi sea.⁴⁴⁻⁴⁶ It was not even necessary that the exciton be a real bound state. A many-body enhancement occurred provided lifetime broadening was not too severe. Close to the threshold, absorption is determined by the change of the scatter-

ing phase shift δ_i of the conduction electrons brought about by the change in the potential due to the presence of the core hole.⁴⁷ Ignoring lifetime broadening effects, the shape of the photoabsorption is

$$\alpha(\omega) \propto (\omega - \omega_0)^{-\alpha_i} \theta(\omega - \omega_0) \quad , \quad (13)$$

where ω is the transition energy, ω_0 is the threshold energy, $\theta(\omega - \omega_0)$ is the unit step function which is zero for $\omega < \omega_0$, and α_i is a critical exponent which depends on the phase shifts. If the critical exponent is positive the threshold is enhanced, and if negative it is suppressed. In fact, Combescot and Nozières⁴⁷ find two thresholds, the enhanced exciton threshold, and a second suppressed threshold corresponding to excitation of an electron to the continuum conduction density of states. Here we are concerned only with the former, the prominent observable feature. The second threshold may be artificial, a consequence of their use of a contact potential. If the second threshold is real, it would be a third possible explanation of the poorly resolved higher-energy structure which we observe.

An important consequence of the theory is that it identifies the x-ray absorption threshold enhancement found in metals, the so called "infrared singularity,"⁴⁸ as being the remains of the exciton threshold. The singularity is thought to be due to the many-body process where the x ray excites an electron to a virtual bound state, accompanied by the infinitesimal excitation (hence "infrared") of an infinite number of electron-hole pairs across the Fermi level. We will refer to this phenomenon

as an x-ray singularity. Starting with the conventional bound-state exciton found in insulators or semiconductors, Combescot and Nozières visualize a continuous transformation to the x-ray singularity as the Fermi level is raised through the gap and on into the conduction band. For the case where the bound state exists, the transformation is accomplished through intermediate stages where the exciton approaches the band edge and broadens asymmetrically toward higher energies, filling in the absorption spectrum gap between the exciton and the continuum.

The amorphous Mg-group-V alloys are an elegant system in which to study this transformation. Excitons exist in the low-conductivity region $x \sim 0.6$, and x can be varied continuously to shift the Fermi level. Also, Mg possesses a typical x-ray singularity at the $L_{II,III}$ edge (Fig. 4). In spite of the approximations of the theory, Eq. (13) seems likely to be a correct description of the photoabsorption near threshold. It is therefore important to extract the critical exponent α_I from the asymmetrically broadened excitons. In this study of the critical exponent we concentrate on $a\text{-Mg}_x\text{Sb}_{1-x}$ since its excitons were observed for a wide range of x . We work with the extracted $\alpha_c(\omega)$ component absorption spectra from Fig. 10, where the background absorption has been subtracted and where the complication of the initial-state spin-orbit splitting has been removed by using the assumptions in Eqs. (5) and (6). This allows the

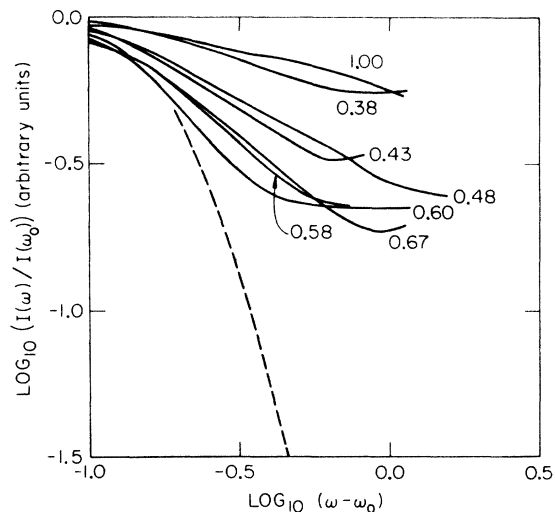


FIG. 12. Logarithmic $a\text{-Mg}_x\text{Sb}_{1-x}$ photoabsorption thresholds. $I(\omega)$ is the absorption coefficient $\alpha(\omega)$ with the background absorption subtracted. Photon energy ω and threshold energy ω_0 are measured in eV. Curves are labeled according to composition x . The dashed curve is the low-energy side of the exciton resonance for $x \sim 0.6$, reflected through the threshold to demonstrate the limitation imposed by the line broadening.

TABLE II. Values for the critical exponent at various alloy compositions. The values labeled α_I^{old} were obtained by a successive approximation application of Eq. (13) to the doublet threshold structure (Ref. 15). Those labeled α_I are regarded as better values, and were obtained from the resolved components of the doublet structure. Uncertainties are about ± 0.1 for α_I .

Composition	α_I^{old}	α_I
Mg	0.35	0.22
$a\text{-Mg}_{57}\text{Bi}_{43}$		0.7
$a\text{-Mg}_{38}\text{Sb}_{62}$	0.18	0.30
$a\text{-Mg}_{43}\text{Sb}_{57}$	0.45	0.63
$a\text{-Mg}_{48}\text{Sb}_{52}$	0.39	0.55
$a\text{-Mg}_{58}\text{Sb}_{42}$	0.51	0.87
$a\text{-Mg}_{60}\text{Sb}_{40}$	0.66	1.04
$a\text{-Mg}_{67}\text{Sb}_{33}$	0.50	0.81

critical exponents α_I to be determined easily using Eq. (13). In Fig. 12 we plot $\log_{10}\alpha_c(\omega)$ vs $\log_{10}(\omega - \omega_0)^{-1}$ for ω above threshold. The curves are labeled according to composition x in $a\text{-Mg}_x\text{Sb}_{1-x}$, except that $x = 1.00$ corresponds to $c\text{-Mg}$. The slopes of the lines give the values of α_I . Their degree of linearity is a measure of how well they fit the theory. The curves with larger α_I values are less linear since the sharper exciton lines show the effect of lifetime broadening more clearly. This broadening limitation is shown by a dashed line in the figure, which is a plot of the $a\text{-Mg}_3\text{Sb}_2$ threshold shape for $\omega < \omega_0$, which should theoretically be sharp. Thus the true α_I values for $x = 0.58$, 0.60 , and 0.67 could conceivably be larger than those obtained experimentally. All of the curves are flat near the $(\omega - \omega_0)^{-1}$ pole because the absorption remains finite at that point (attributed to conduction electron interaction). Also, all of the curves become level around 1 eV above threshold where transitions to the band density of states become increasingly important.

We have previously published values of α_I determined manually from a successive approximation application of Eq. (13) to the unresolved threshold doublet structure.¹⁵ These values are listed in Table II, together with better values obtained by computer analysis of the component spectra. The qualitative behavior is still the same. As predicted by theory, α_I is a maximum for the most insulating composition. As x changes from 0.6, the alloy becomes more metallic and both the resistivity and α_I decrease, as is shown in Fig. 13. For the extremes of composition $x = 0.38$ and 0.67 , the shape of the asymmetric broadening (Fig. 10) tends toward the shape seen in pure Mg, which supports the interpretation that the metallic x-ray singularity is a kind of Auger-broadened exciton remnant.

We have followed the exciton to low concentrations of Bi, $x = 0.9$, where it disappeared. This

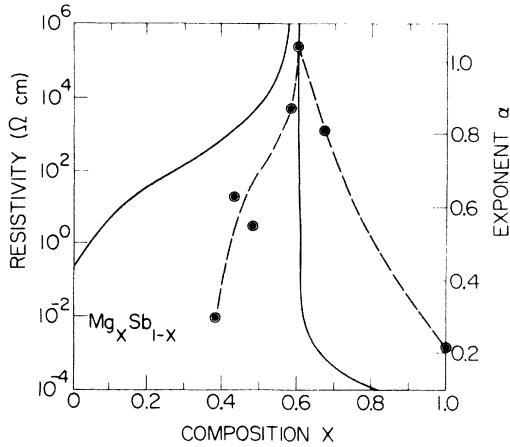


FIG. 13. Resistivity and critical exponents of $\alpha\text{-Mg}_x\text{Sb}_{1-x}$. The solid curve (log scale on the left) shows resistivity of $\alpha\text{-Mg}_x\text{Sb}_{1-x}$ at 273 K from Ref. 10, as a function of composition x . Critical exponents are indicated by data points with dashed curve, and linear scale on the right. The point at $x=1.0$ is for $c\text{-Mg}$.

disappearance is not conclusive evidence that the exciton ever disappears in amorphous alloy, however, since such samples were probably microcrystalline, as mentioned earlier. The exciton resonance was absent for all compositions of $c\text{-Mg}_x\text{Bi}_{1-x}$ alloys.

It is unclear why excitons were not observed in $c\text{-Mg}_3\text{Bi}_2$. There is still oscillator strength which can be identified as belonging to excitation of the Mg $2p$ electron. This is best seen in spectrum B of Fig. 5, and less well in Fig. 7. The resonances were still quite strong in $\alpha\text{-Mg}_{75}\text{Bi}_{25}$ ($\sigma = 2 \times 10^3 \Omega^{-1} \text{cm}^{-1}$), but absent in $c\text{-Mg}_3\text{Bi}_2$ ($\sigma = 7 \times 10^2 \Omega^{-1} \text{cm}^{-1}$). Screening probably cannot provide a complete explanation. The wave functions are more localized in the absence of long-range order, and this should enhance the transition matrix element. Also, since Mg_3Bi_2 is a semimetal, or possibly a very degenerate semiconductor, the Fermi level must lie near the band edge. When this happens, it has been indicated⁴⁷ that in the absence of a bound state, all δ_i become zero and the singularity disappears. One would be left with a step function, possibly broadened by the increased screening. In that case the phase transition would be the cause of a change in the nature of the critical exponent, from 1 to 0, due to a change in the density of states from a pseudogap of localized states to semimetallic overlapping bands of extended states.

Although we have not examined crystalline Mg_3Sb_2 , it is a semiconductor with a band gap of 0.82 eV, and all arguments lead us to expect that the excitons should persist when $\alpha\text{-Mg}_3\text{Sb}_2$ crystallizes.

B. Ionicity

We have noted that the excitons in $\alpha\text{-Mg}_x\text{Sb}_{1-x}$, as compared to those in $\alpha\text{-Mg}_x\text{Bi}_{1-x}$, were (i) more broadened for $x \sim 0.6$, (ii) further shifted toward higher energy from the threshold transition of pure Mg, and (iii) stronger, as measured by their line intensities. To compare these differences quantitatively, we define and tabulate the parameters Γ , E_B , E_D , δE , and A .

For the asymmetrically broadened component spectra in Figs. 6 and 10, the parameter Γ is twice the difference between the energy where the absorption peak occurs, and the lower energy where the absorption is half as strong. For a symmetric line, Γ would simply be the half-width. For the thresholds with which we are dealing, we measure Γ in this different way to get a true measure of lifetime broadening, uncomplicated by higher-order structure or asymmetric broadening.

The parameters E_B and E_D are energy values which correspond to the positions of the threshold energies E_C and E_A respectively, if the shifting effect of the electron-hole exchange interaction is extracted. E_B and E_D are also the energies of the forbidden transitions to the pure triplet states which have total electron-hole angular momenta $J=2, 0$ respectively, because, since these optical transitions are forbidden, the positions of these final states are unaffected by exchange interaction.³⁴ It is proper to compare E_B and E_D with the L_{III} and L_{II} thresholds, respectively, of pure Mg, since they are in fact the L_{III} and L_{II} energies for an alloy or ionized state of Mg. E_B and E_D are used here to compare chemical shifts caused by differing numbers of conduction electrons in the vicinity of the Mg atom.⁴⁹ The energies of these levels are related to the allowed transitions by³⁴

$$\begin{pmatrix} E_B \\ E_D \end{pmatrix} = \frac{E_A + E_C}{2} - \frac{\Delta \pm \lambda}{2}, \quad (14)$$

where Δ and λ are obtained from Eqs. (1) and (2). We also introduce the parameter δE which measures the chemical shift of these levels in any ionic state of Mg relative to the $L_{II, III}$ levels in Mg metal. In Mg metal, $\delta E = 0$ by definition. The opposite extreme is the maximum ionization state of Mg likely to be found in solids, Mg^{2+} . As reference points we take values of E_B , E_D , and δE for Mg^{2+} from data for the free ion, Mg III .³²

The final parameter A is proportional to the total oscillator strength of the Mg $2p \rightarrow$ threshold transition, evaluated at threshold:

$$A = \sum_i \Gamma_i \alpha_i^{\text{max}} = \Gamma \alpha_C^{\text{max}} (1 + I_A/I_C), \quad (15)$$

where the summation is over the allowed transitions and α^{max} is the absorption coefficient mea-

TABLE III. Threshold parameters for excitation of Mg $2p$ electrons. The least ionic state of Mg is at the top. Ionicity generally increases for Mg in compound with Bi, Sb, Br, Cl, and F. Mg^{2+} represents the maximum likely ionic state of Mg in compound. Data for Mg halides are calculated from data in Ref. 35. Data for Mg^{2+} are from Ref. 32.

Composition	Half-width Γ (eV)	L_{III} thresh. E_B (eV)	L_{II} thresh. E_D (eV)	Chem. shift δE (eV)	Strength A (10^4 eV/cm)
Mg	0.1	49.46	49.71	0	2.2
a -Mg ₅₇ Bi ₄₃	0.17	50.82	51.11	1.38	2.6
a -Mg ₆₀ Bi ₄₀	0.2	50.8	51.1	1.3	5
a -Mg ₃₈ Sb ₆₂	0.5	50.95	51.28	1.5	3.8
a -Mg ₄₃ Sb ₅₇	0.38	51.05	51.35	1.62	5.6
a -Mg ₄₈ Sb ₅₂	0.39	51.17	51.46	1.73	6.9
a -Mg ₅₈ Sb ₄₂	0.30	51.18	51.47	1.74	6.4
a -Mg ₆₀ Sb ₄₀	0.30	51.17	51.45	1.73	7.6
a -Mg ₆₇ Sb ₃₃	0.36	51.12	51.40	1.68	3.6
MgBr ₂	0.20 ^a	53.03	53.30	3.58	
MgCl ₂	0.31 ^a	53.49	53.80	4.06	
MgF ₂	0.57 ^a	53.73	54.13	4.35	
Mg^{2+}		52.76	53.03	3.31	

^aAverage value.

sured above background at the energy corresponding to maximum transition threshold oscillator strength.

Values of these parameters, as determined in c -Mg, a -Mg _{x} Bi _{$1-x$} , and a -Mg _{x} Sb _{$1-x$} , are listed in Table III. For comparison, data are also listed for Mg^{2+} (Ref. 32) and Mg halides.³⁵ As mentioned earlier, the oscillator strength of the threshold transition is greater in a -Mg₃Sb₂ than in a -Mg₃Bi₂. Using the parameter A , the transition is 1.5 times stronger in the Sb alloy. This was attributed to a matrix element effect, since the lowest unoccupied state is expected to have a more s -like admixture in a -Mg₃Sb₂. Within the a -Mg _{x} Sb _{$1-x$} system, the variation of threshold transition strength reaches a maximum at $x=0.6$, due to minimum screening, as discussed earlier.

The value of the chemical shift δE correlates with the ionicity of the Mg atom. Coulson and Zauli have found a quadratic relationship between the chemical shift and ionicity in sulfur.⁴⁹ Defining $\delta E = 0$ in Mg metal, a value near $\delta E = 3.31$ eV would indicate that an Mg atom in compound is in the Mg^{2+} state. It is seen from Table III that Mg-Sb alloys are noticeably more ionic than Mg-Bi alloys, but that neither is as truly ionic as are the Mg halides. The δE values for the halides were calculated from E_C and E_A values which had not been corrected for background, nor for the mutual distortion caused by the lines being close to each other in energy. Therefore, we regard the E_C and E_A values for the halides as being approximate.

The fact that a -Mg _{x} Sb _{$1-x$} is more ionic than a -Mg _{x} Bi _{$1-x$} is in agreement with both their electrical conductivity differences,^{10,17} and with the difference in the heats of formation between Mg₃Sb₂

and Mg₃Bi₂, 16 vs 7.4 kcal/mole.⁵⁰ Likewise, trends in ionicity occur within the a -Mg _{x} Sb _{$1-x$} system. In this case the ionicity is maximum for $x=0.6$, and decreases for an excess of Mg or Sb. This suggests that an excess of either constituent increases the number of carriers at finite temperature by shifting the Fermi level through the pseudogap toward a density of extended states. This agrees with thermoelectric power measurements which indicate that the Fermi level rises through the pseudogap as the Mg concentration is increased.¹⁷

The half-width Γ also depends on ionicity and the number of carriers near the Mg atom, as long as we remain within a particular alloy system. In a -Mg _{x} Sb _{$1-x$} , for example, the Mg atom is most ionic when $x=0.6$. The screening and the Coulomb broadening due to other electrons is a minimum at $x=0.6$, so the exciton lifetime is a maximum and the lines are narrowest. Comparing the Sb and Bi alloys, it is necessary to realize that the exciton lifetimes depend on the competition between the Coulomb binding potential and the repulsive overlap of the electrons associated with Bi or Sb. To explain why Γ is narrower in the less ionic Bi alloy one could examine the width of the Mg to heavy-atom hopping transition using wave functions like those found in the tables of Herman and Skillman.⁵¹ Here we only note that the trend of Γ to decrease as the anion atomic weight increases appears to be true for both group-V and group-VII anions.

VI. CONCLUSION

Core excitons have been identified in amorphous Mg alloys as giving rise to sharp photoabsorption structure in the soft-x-ray region. We have examined the absorption spectra using several sim-

ple physical principles to obtain information about the short-range interactions in the amorphous solid. The strength of the exciton threshold transition depends on the final-state symmetry and the effectiveness of screening. There was considerable shifting of oscillator strength between the components of the threshold spin-orbit doublet, attributed to exchange interaction. The magnitude of the exchange interaction indicates that the exciton is compact. The chemical shifting of the transition threshold energy allows us to order the ionicities of Mg atoms in various compounds on a relative scale. Within an alloy system, the small shift in line or threshold position, and small changes in half-width, vary continuously with conductivity and may relate to changing ionicities in the alloys.

There appeared to be some higher-energy structure just above the photoabsorption threshold. If this is an envelope of an $n > 1$ exciton series, an upper limit on the $n=1$ exciton radius would be around 3 \AA in $a\text{-Mg}_3\text{Bi}_2$. The exciton is screened for screening lengths comparable to this ($2\text{--}6 \text{ \AA}$ as estimated from conductivity data). Strong absorption between $60\text{--}80\text{-eV}$ photon energy, due to delayed $d\text{--}f$ resonances, made it desirable to use thin samples. While the $n=1$ exciton line was independent of thickness for thicknesses greater than 100 \AA , higher order excitons have larger radii, and may have been suppressed.⁵² These $n > 1$ excitons should be sought in samples thicker than 500 \AA to see if higher energy structure can be better resolved, but the large ratio of background absorption to their weaker structure is likely to make such study difficult. This simple interpretation is advanced with some caution, however, since band absorption, a multiple excitation process, or other channels of excitation may be responsible for the observed structure. Furthermore, although we use the term "exciton," it seems that an accurate many-body treatment is necessary instead of a simple single process explanation, particularly for the more metallic compositions. The simpli-

fied model of Combescot and Nozières is a step in this direction. The shape of the exciton lines was approximately described by a critical exponent, such as appears in their model. It is important that the exciton line shape can be followed continuously from insulating to metallic conductivity, varying from a sharp resonance to the type of singularity observed in metals. The ability to follow these phenomena depends on an unusual property of the amorphous Mg-Bi and Mg-Sb alloy systems, that by controlling composition one can move the Fermi level through the pseudogap and into the conduction band of extended states. During the transition from metallic to insulating behavior, both the screening and the critical exponent vary qualitatively together, since both depend on the response of the conduction electrons to the excitation process. It is remarkable that the excitons exist in spite of the probable absence of a true gap in the density of states, a mobility gap or pseudogap containing only localized states being sufficient. No temperature dependence of the exciton linewidth was noted in Mg_3Bi_2 films except that the sharp exciton resonances disappeared when the films were crystallized.

ACKNOWLEDGMENTS

The author expresses his appreciation to F. C. Brown for guidance throughout this research. He also thanks E. A. Davis, J. D. Dow, C. Gähwiler, A. B. Kunz, O. Rustgi, W. C. Scheifley, and B. Sonntag for assistance and many useful conversations. E. M. Rowe and the storage-ring staff at the University of Wisconsin Physical Science Laboratory, Stoughton, Wisc., were most generous with their time during the data-gathering phase of this work. Finally, the author thanks R. Anderson for micrographs and electron diffraction studies of the Mg-Bi samples, D. Read for micrographs and diffraction patterns of Mg-Sb samples and J. B. Woodhouse for electron microprobe analysis of Mg-Bi samples.

*Research supported in part by the U. S. Army Research Office under Contract No. ARO-D-31-124-71-G15, the Advanced Research Projects Agency under Contract No. HC15-67-C-0021, and the National Science Foundation under Grant No. NSF-GH-33634.

†Work performed in partial fulfillment of the requirements for the Ph.D. degree. Present address: Xerox Corporation, Webster Research Center, Webster, N. Y. 14580.

¹Y. Cauchois and N. F. Mott, *Philos. Mag.* **40**, 1260 (1949).

²B. Raz and J. Jortner, *Proc. R. Soc. A* **317**, 113 (1970).

³B. Raz, A. Gedanken, U. Even, and J. Jortner, *Phys. Rev. Lett.* **28**, 1643 (1972).

⁴J. L. Hartke and P. J. Regensburger, *Phys. Rev.* **139**,

A 970 (1965).

⁵N. F. Mott and E. A. Davis, *Electronic Processes in Non-crystalline Materials* (Oxford U. P., New York, 1971).

⁶F. Seitz, *Modern Theory of Solids* (McGraw-Hill, New York, 1940), p. 74.

⁷V. P. Zhuze, I. V. Mochan, and S. M. Ryvkin, *Zh. Tekh. Fiz.* **18**, 1494 (1948).

⁸B. I. Boltaks and V. P. Zhuze, *Izv. Akad. Nauk. SSSR, Ser. Fiz.* **16**, 155 (1952).

⁹G. Busch, F. Hulliger, and U. Winkler, *Helv. Phys. Acta* **27**, 249 (1954).

¹⁰R. P. Ferrier and D. J. Herrell, *J. Non-Cryst. Solids* **2**, 278 (1970).

¹¹B. I. Boltaks and V. P. Zhuze, *Zh. Tekh. Fiz.* **18**,

- 1459 (1948).
- ¹²T. S. Moss, Proc. Phys. Soc. B 63, 982 (1950).
- ¹³F. C. Brown, in *Solid State Physics*, edited by H. Ehrenreich, F. Seitz and D. Turnbull (Academic, New York, to be published), Vol. 29.
- ¹⁴J. H. Slowik and F. C. Brown, Bull. Am. Phys. Soc. 17, 366 (1972).
- ¹⁵J. H. Slowik and F. C. Brown, Phys. Rev. Lett. 29, 934 (1972).
- ¹⁶C. Kunz, R. Haensel, G. Keitel, P. Schreiber, and B. Sonntag, in *Electronic Density of States*, edited by L. H. Bennett, U. S. Natl. Bur. Stds. Spec. Publ. No. 323 (U. S. GPO, Washington, D. C., 1971), p. 323.
- ¹⁷R. P. Ferrier and D. J. Herrell, Philos. Mag. 19, 853 (1969).
- ¹⁸R. P. Ferrier and D. J. Herrell, J. Non-Cryst. Solids 4, 338 (1970).
- ¹⁹C. J. Smithells, *Metals Reference Book*, 4th ed. (Plenum, New York, 1967), Vol. 2.
- ²⁰H. H. A. Bath and W. Steckelmacher, J. Sci. Instrum. 42, 144 (1965).
- ²¹S. Tolansky, Nature (Lond.) 152, 722 (1943).
- ²²J. E. Enderby and E. W. Collings, J. Non-Cryst. Solids 4, 161 (1970).
- ²³S. Mader, A. S. Nowick, and H. Widmer, Acta Met. 15, 203 (1967).
- ²⁴G. Bergman, Phys. Rev. B 7, 4850 (1973), and papers cited therein.
- ²⁵F. C. Brown, P. L. Hartman, P. G. Kruger, B. Lax, R. A. Smith, and G. H. Vineyard, National Research Council Solid State Panel Subcommittee Report, March, 1966 (unpublished).
- ²⁶R. Haensel and C. Kunz, Z. Angew. Phys. 23, 276 (1967).
- ²⁷C. Gähwiller, F. C. Brown, and H. Fujita, Rev. Sci. Instrum. 41, 1275 (1970).
- ²⁸F. C. Brown, C. Gähwiller, H. Fujita, A. B. Kunz, W. Scheifley, and N. Carrera, Phys. Rev. B 2, 2126 (1970).
- ²⁹R. W. G. Wyckoff, *Crystal Structures* (Interscience, New York, 1948).
- ³⁰F. A. Shunk, *Constitution of Binary Alloys, Second Supplement* (McGraw-Hill, New York, 1969).
- ³¹N. J. Shevchik, J. Tejada, D. W. Langer, and M. Cardona, Phys. Rev. Lett. 30, 659 (1973).
- ³²C. E. Moore, *Atomic Energy Levels*, U. S. Natl. Bur. Stds. Circ. No. 467 (U. S. GPO, Washington, D. C., 1949), p. 109.
- ³³J. A. Bearden and A. F. Burr, Rev. Mod. Phys. 39, 125 (1967).
- ³⁴Y. Onodera and Y. Toyozawa, J. Phys. Soc. Jap. 22, 833 (1967).
- ³⁵P. Rabe, B. Sonntag, T. Sagawa, and R. Haensel, Phys. Status Solidi B 50, 559 (1972).
- ³⁶R. Haensel, C. Kunz, and B. Sonntag, Phys. Lett. A 25, 205 (1967).
- ³⁷J. M. Ziman, *Principles of the Theory of Solids* (Cambridge U. P., Cambridge, England, 1965), p. 131.
- ³⁸R. J. Elliott, Phys. Rev. 108, 1384 (1957).
- ³⁹D. L. Dexter and R. S. Knox, *Excitons* (Wiley, New York, 1965), p. 52.
- ⁴⁰H. Haken, Fortsch. Phys. 6, 271 (1958).
- ⁴¹J. Ringeissen, A. Coret, and S. Nikitine, in *Localized Excitations in Solids*, edited by R. F. Wallis (Plenum, New York, 1968), p. 297.
- ⁴²J. C. Hermanson, Phys. Rev. 177, 1234 (1969).
- ⁴³Y. Toyozawa, Prog. Theor. Phys. 20, 53 (1958).
- ⁴⁴G. D. Mahan, Phys. Rev. 153, 882 (1967).
- ⁴⁵G. D. Mahan, Phys. Rev. Lett. 18, 448 (1967).
- ⁴⁶G. D. Mahan, Phys. Rev. 163, 612 (1967).
- ⁴⁷M. Combescot and P. Nozières, J. Phys. (Paris) 32, 913 (1971).
- ⁴⁸J. J. Hopfield, Commun. Solid State Phys. 2, 40 (1969).
- ⁴⁹C. A. Coulson and C. Zauli, Molec. Phys. 6, 525 (1963).
- ⁵⁰J. H. Westbrook, *Intermetallic Compounds* (Wiley, New York, 1967), p. 45.
- ⁵¹F. Herman and S. Skillman, *Atomic Structure Calculations* (Prentice-Hall, Englewood Cliffs, N. J., 1963).
- ⁵²R. A. Satten and S. Nikitine, Phys. Cond. Matter 1, 394 (1963).